

Assessment of Intrathoracic Airway Trees: Methods and In Vivo Validation

Kálmán Palágyi^{1,2}, Juerg Tschirren², Eric A. Hoffman³, and Milan Sonka²

¹ Dept. of Image Processing and Computer Graphics,
University of Szeged, H-6720 Szeged, Hungary
`palagyi@inf.u-szeged.hu`

² Dept. of Electrical and Computer Engineering,
The University of Iowa, Iowa City IA 52242, USA
{`juerg-tschirren,milan-sonka`}@uiowa.edu

³ Dept. of Radiology,
The University of Iowa, Iowa City IA 52242, USA
`eric-hoffman@uiowa.edu`

Abstract. A method for quantitative assessment of tree structures is reported allowing evaluation of airway tree morphology and its associated function. Our skeletonization and branch-point identification method provides a basis for tree quantification or tree matching, tree-branch diameter measurement in any orientation, and labeling individual branch segments. All main components of our method were specifically developed to deal with imaging artifacts typically present in volumetric medical image data. The proposed method has been tested in a computer phantom subjected to changes of its orientation as well as in repeatedly CT-scanned rigid and rubber plastic phantoms. In this paper, validation is reported in six in vivo scans of the human chest.

1 Introduction

Tubular structures are frequently found in living organisms. The tubes – e.g., arteries or veins are frequently organized into more complex structures. Trees consisting of tubular segments form the arterial and venous systems, intrathoracic airways form bronchial trees, and other examples can be found. Computed tomography (CT) or magnetic resonance (MR) imaging provides volumetric image data allowing identification of such tree structures. Frequently, the trees represented as contiguous sets of voxels must be quantitatively analyzed. The analysis may be substantially simplified if the voxel-level tree is represented in a formal tree structure consisting of a set of nodes and connecting arcs. To build such formal trees, the voxel-level tree object must be transformed into a set of interconnected single-voxel centerlines representing individual tree branches. Therefore, the aim of our work was to develop a robust method for identification of centerlines and bifurcation (trifurcation, etc.) points in segmented tubular tree structures acquired in vivo from humans and animals using volumetric CT or MR scanning, rotational angiography, or other volumetric imaging means.

Many researchers focused on this task in the past [2,3,6,7,8,11,13,14]. Despite of the wealth of previous work, no perfect skeletonization technique exists to date. Our new approach that is presented below is attempting to overcome most of the existing problems. Since our work is driven by the need for quantitative analysis of intrathoracic airway trees from multidetector CT images, we concentrated on developing a method serving this purpose. However, the resulting approach is widely applicable to a variety of medical image data.

2 Methods

The reported method allows to quantitatively analyze tubular tree structures. Assuming an imperfectly segmented tree was obtained from volumetric data in the previous stages, the presented technique allows to obtain a single-voxel skeleton of the tree while overcoming many segmentation imperfections, yields formal tree representation, and performs quantitative analysis of individual tree segments on a tree-branch basis. The input of the proposed method is a 3D binary image representing a segmented voxel-level tree object. All main components of our method were specifically developed to deal with imaging artifacts typically present in volumetric medical image data. As such, the method consists of the following main steps:

1. *Topological correction of the segmented tree*: Internal cavities (i.e., connected “0” voxels surrounded by “1” voxels), holes (i.e., “0” voxels forming tunnels), and bays (i.e., disturbances without a topological change) are eliminated by sequential forward and backward scanning (instead of the conventional object labeling) and morphological closing.
2. *Identification of the tree root*: In the pulmonary CT images, the center of the topmost nonzero 2D slice in direction z (detected by 2D shrinking) defines the root of the formal tree to be generated and belongs to the trachea. The detected root voxel acts as an anchor point during the centerline extraction (i.e., it cannot be deleted by the forthcoming iterative peeling process).
3. *Extraction of the 3D centerlines – skeletonization*: A sequential 3D curve-thinning algorithm was developed for extracting both geometrically and topologically correct centerlines.
4. *Tree pruning*: False segments are removed by using both the length and depth information.
5. *Identification of branch points*: In a centerlines, three types of points can be identified: endpoints (which have only one 26-neighbor [5]), line-points (which have exactly two 26-neighbors), and branchpoints (which have more than two 26-neighbors) that form junctions (bifurcations, trifurcations, etc.).
6. *Generation of a formal tree structure*: The centerlines are converted into a graph structure (each voxel corresponds to a graph node/vertex and there is an edge between two nodes if the corresponding voxels are 26-adjacent. A similar structure is assigned to the branchpoints. In the branch-tree, a path between two branch- or endpoints is replaced by a single edge.

7. *Tree partitioning*: All voxels of the elongated binary tree (after the topological correction) are partitioned into branches — each voxel is assigned a branch-specific label. A gray-level image is created, in which value “0” corresponds to the background and different non-zero values are assigned to the voxels belonging to different tree branches/partitions.
8. *Calculating associated measures*: For each partition/branch of the tree, the following quantitative indices are calculated: branch length, branch volume, branch surface area, and branch radius.

The entire process has been described in [9,10], therefore, only the critical steps are now described in more detail.

2.1 Centerline Extraction

One of the well-known approaches to centerline determination is to construct a 3D skeleton of the analyzed object. However, some of the properties of 3D skeletons in discrete grids are undesirable. Specifically, in the case of 3D tubular objects, we do not need the exact skeleton, since a 3D skeleton generally contains surface patches. We need a skeletonization method that can suppress creation of such surface patches. As a solution, a 3D curve-thinning algorithm was developed that is preserving line-end points and can thus extract both geometrically and topologically correct centerlines. As part of this process, a novel method for endpoint re-checking was developed based on comparisons between the centerline configuration at some stage of thinning and the previous object configuration.

Thinning is a frequently used method for producing an approximation to the skeleton in a topology-preserving way [5]. Border points of a binary object that satisfy certain topological and geometric constraints are deleted in the iteration steps. In case of tubular 3D objects, thinning has a major advantage over other skeletonization methods. Curve-thinning (i.e., iterative object reduction preserving line-end points) can directly produce one voxel wide centerlines.

We proposed a sequential curve-thinning algorithm [9,10]. One iteration step of the object reduction process is decomposed into six successive sub-iterations according to the six main directions in 3D. Each sub-iteration consists of two phases; at first the border points according to the actual deletion direction that are simple (i.e., their deletion does not alter the topology of the image [5]) and not line-end points are marked as potential deletable. Then marked points are checked: a marked point is deleted if it remains simple and is not a line-end point after the deletion of some previously visited marked points. In addition, in some special cases, simple points are also deleted if they have become line-end points. That endpoint re-checking process statistically decreases the number of unwanted/false side branches in the created centerlines [10].

It can produce maximally thinned (i.e., 1-voxel wide) centerlines (see Fig. 1, since all simple points are deleted). The produced centerline is topologically equivalent to the original elongated object, since simple points are deleted sequentially. Our algorithm is topology-preserving by definition of simple points, therefore, the proof is self-evident.

Additionally, our method allows an easy and efficient implementation. It is much faster than the thinning algorithms employed, e.g., in [13].

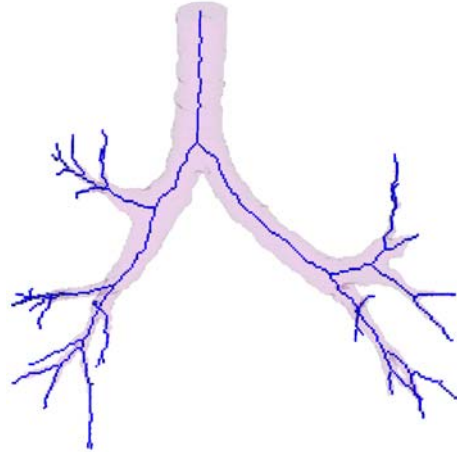


Fig. 1. The segmented volume of a human airway tree and its centerlines extracted by the proposed curve–thinning algorithm

2.2 Pruning

Unfortunately, each skeletonization algorithm (including ours) is rather sensitive to coarse object boundaries or surfaces. As a result, the produced (approximation to the) skeleton generally includes false segments that must be removed by a pruning step. Applying a proper pruning method that would yield reliable centerlines is critical in all tree-skeletonization applications. An unwanted branch causes false generation numbering and consequently false measurements corresponding to the individual segments of the tree (including length, volume, surface area, etc.).

We have developed a centerline pruning that uses both the branch length and the distance-from-surface (depth) information for the identification of the following pruning candidate: all branches are deleted if their lengths are shorter than a given threshold t_l and their associated branchpoints are not closer to the border/surface of the elongated tree (after topological correction) than a given threshold t_d :

The pruning process can be repeated for different pairs of thresholds (t_l, t_d) . In our experience, 2 to 4 iterations typically provide satisfactory results for in vivo airway trees. The result of our pruning is demonstrated in Fig. 2.

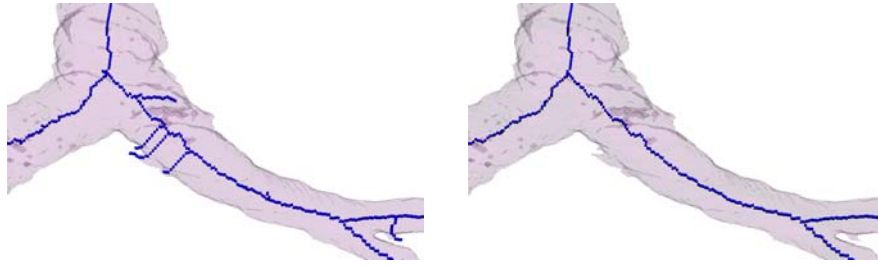


Fig. 2. A part of a segmented tree and its centerline before pruning (left) and after pruning (right). The applied pruning technique can delete unwanted long branches from thick parts and unwanted shorter ones from thinner parts, while correct branches are typically preserved throughout the tree

2.3 Tree Partitioning

The aim of the partitioning procedure is to partition all voxels of the binary tree into branches — each voxel is assigned a branch-specific label. There are two inputs into the process — the binary image after topological corrections, and the formal tree structure corresponding to the centerlines. The output is a gray-level image, in which value “0” corresponds to the background and different non-zero values are assigned to the voxels belonging to different tree branches/partitions (Fig. 3).

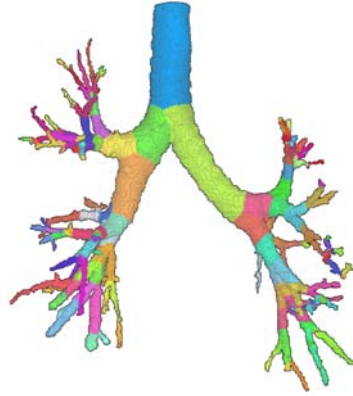


Fig. 3. The the partitioned volume of a human airway tree close to total lung capacity (TLC)

The automated partitioning consists of two steps. First, only the voxels in the centerlines are partitioned so that each branch/partition of the centerlines has a unique label. Non-skeletal tree voxels are then partitioned by isotropic

label propagation — each voxel in the tree gets the label of the closest skeletal point.

2.4 Calculating Associated Measures

For each partition/branch of the tree, the following measures/indices are calculated:

- branch length — defined as a Euclidean distance between the parent and child branchpoints (in *mm*),
- branch volume — defined as a volume of all voxels belonging to the branch (in *mm*³),
- branch surface area — defined as a surface area of all boundary voxels belonging to the branch (in *mm*²),
- branch radius — derived from the branch length and the branch volume assuming “cylindrical” partition (in *mm*):

$$radius = \sqrt{\frac{volume}{\pi \cdot length}}.$$

Determining the first three indices is fairly straightforward, but calculating a reliable approximation to the branch radius is rather complicated. The two ends of a partition/branch are “conic”, therefore, they must be suppressed to get measurements only from the “cylindrical” partitions.

3 Experimental Methods

Performance of the reported method was assessed in 343 computer phantom instances subjected to changes of its orientation, in a rigid plastic phantom CT-scanned under 9 orientations, in a rubber plastic phantom CT-scanned under 9 orientations, and in six in vivo scans of human lungs.

3.1 Phantoms

The computer phantom [4] is a 3-dimensional structural model of the human airway tree (Fig. 4a). The model consists of 125 elongated branches and its centerlines have 62 branchpoints and 64 endpoints (including the root of the tree) — all positions of the branchpoints are known. The generated object is embedded in a $300 \times 300 \times 300$ binary array containing unit-cube voxels. Independently, the phantom was rotated in 5 degree steps between -15 and $+15$ degrees along all three axes.

The second phantom is a hollow rigid plastic one (Fig. 4b), derived from an in vivo scanned human bronchial tree, transformed in a computer graphics representation, and built by a rapid prototyping machine. The third phantom is a hollow rubber plastic one (Fig. 4c), casted from a normal human bronchial tree

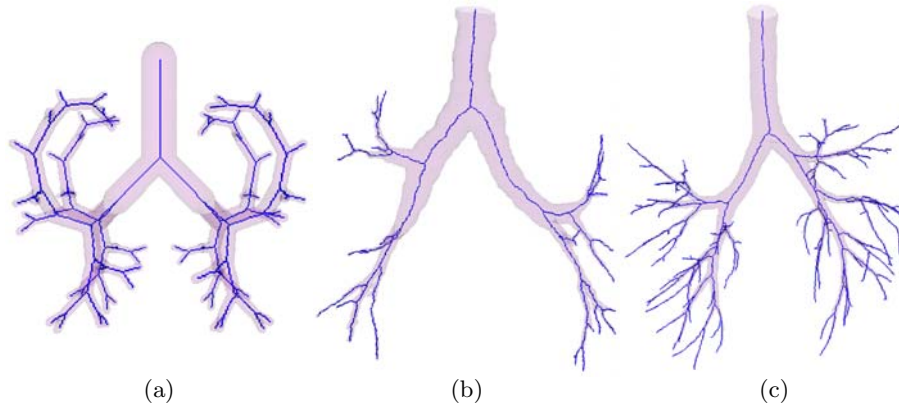


Fig. 4. The computer phantom (a), the rigid phantom (b), and the rubber phantom (c) in their neutral orientations and their centerlines

and consists of about 400 branches and 200 branchpoints. The physical phantom was embedded in potato flakes (simulating lung tissue). The rigid and the rubber phantoms were imaged in 9–9 orientations using multi-row detector computed tomography (4-slice spiral CT, Mx8000, Philips Medical Systems) with voxel size $0.439 \times 0.439 \times 0.5$ mm and $0.488 \times 0.488 \times 0.5$ mm, respectively. The volume sizes were $512 \times 512 \times 300 - 400$ and $512 \times 512 \times 500 - 600$ voxels, respectively. The rotation angles defined 9–9 phantom orientations in the scanner, the orientations were separated by 15° intervals in the $x - z$ and $y - z$ planes.

From the 9–9 CT phantom images, segmentation was performed to separate bronchial airways from the lung parenchyma yielding a binary image used as an input to the reported skeletonization algorithm. For each of the $342 + 9 + 9 = 360$ phantom trees, skeletonization was performed fully automatically and the resulting skeletons were not interactively edited. For each instance of the computer phantoms, the branchpoint position error was determined. It was defined as a Euclidean distance between the skeletonization-determined and true coordinates of the corresponding branchpoints.

For a subset of 9 computer phantoms, the 9 rigid and the 9 rubber phantoms, the above introduced quantitative indices were determined for the first 5 generations of the matched trees. Here, the reproducibility was determined by assessing differences between the reference tree and the tree analyzed in different orientations, after registering the analyzed tree with the reference tree. The quantitative measurements described above were compared in different orientations.

3.2 In Vivo CT Scans

The method was tested in six in vivo scans of the human chest. For each subject, a scan close to total lung capacity (TLC) was acquired by multi-detector row spiral computed tomography with voxel size $0.683 \times 0.683 \times 0.6$ mm³ (4-slice spiral CT,

Mx8000, Philips Medical Systems). The volume sizes were $512 \times 512 \times 450 - 550$ voxels. The segmented in vivo trees are not isometric (i.e., the voxels are cuboids instead of cubes) and contain numerous “thin” branches. To facilitate reproducibility assessment, a “more regular” reference tree was constructed for each segmented subject (see Figs. 5-6). The reproducibility analysis was performed in the reference trees artificially rotated in 8 different ways.

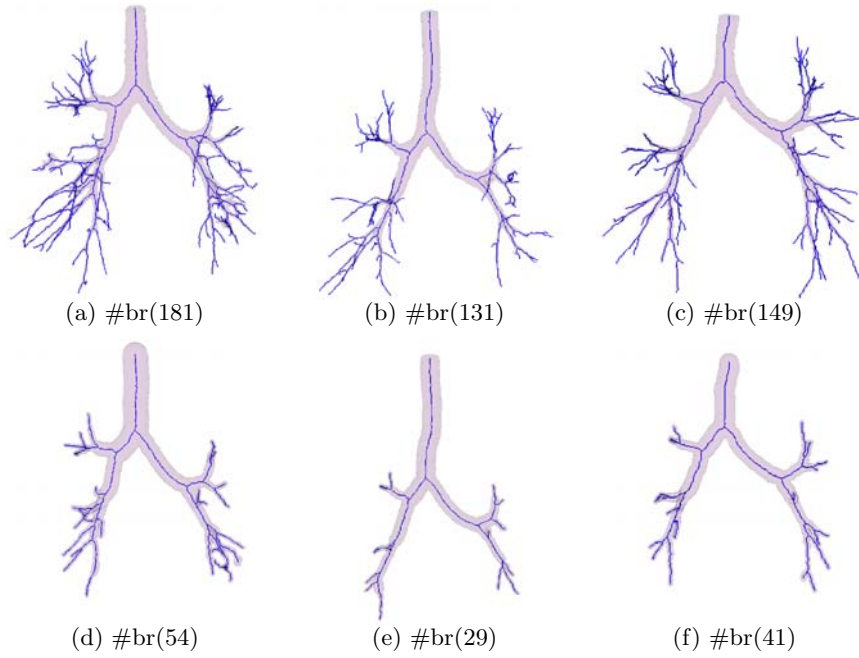


Fig. 5. The first three in vivo TLC trees (a-c) and the corresponding reference trees (d-f) (#br means the number of branches)

The reference tree construction consisted of the following steps:

- Centerlines from the segmented in vivo tree were extracted and the formal tree structure with the associated measures was created. Let S be the set of the skeletal voxels and let $radius(s)$ denote the radius of the branch containing $s \in S$ (in voxel).
- A new tree $R_t(S)$ is formed in the following way:

$$R_t(S) = \bigcup_{s \in S, radius(s) > t} \{ r \mid d(r, s) \leq radius(s) \},$$

where $t \geq 0$ is an integer threshold for suppressing “thin” branches and $d(r, s)$ denotes the Euclidean distance between r and s (in voxel).

In other words, the reference tree is a collection of spheres in which the center of each sphere is a skeletal voxel in a “thick” branch of the original tree and the radius of a sphere is derived from the (cylindrical) radius associated with the corresponding branch of the original tree. Note, that the dimensions of the original and the reference volumes are the same and the reference volume is isometric (unit cube voxels 1 mm^3).

The extraction of the centerlines from each segmented tree was driven by the same pruning parameters. For each of the 6 in vivo trees, skeletonization was performed fully automatically and the resulting skeletons were not interactively edited. Each of the 6 reference trees was created by the same thickness parameter ($t = 2$). Figs. 5-6 show the original and reference trees and their centerlines. Note, that the reference trees are “more cylindrical” and contain much smaller number of branches than the original ones.

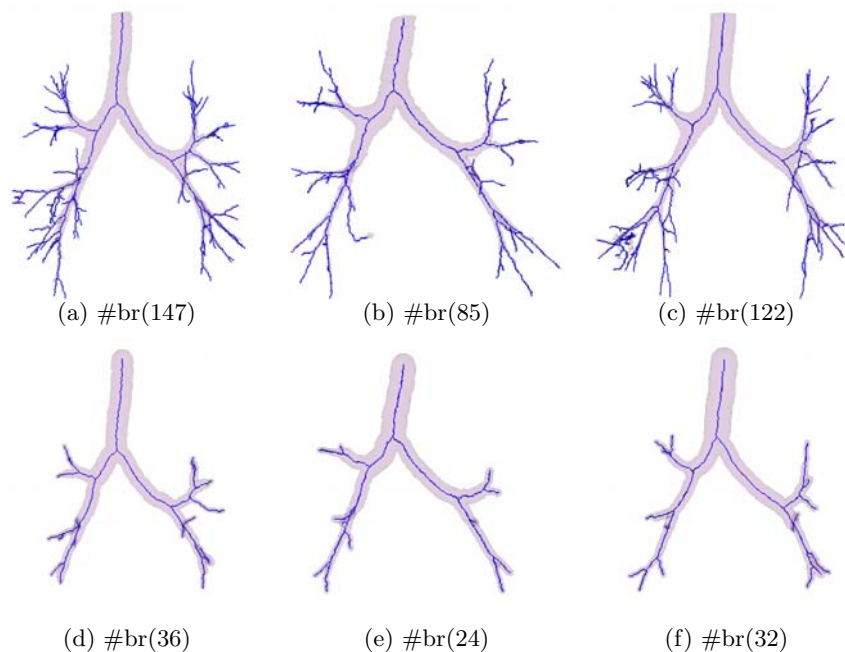


Fig. 6. The last three in vivo TLC trees (a-c) and the corresponding reference trees (d-f) (#br means the number of branches)

For each reference tree, 8 rotated instances were created, the orientations were separated by 15° intervals in the $x - z$ and $y - z$ planes. For each of the 6 trees, a set of 9 trees (i.e., the reference tree in neutral position and its 8 rotated instances), skeletonization and quantitative analysis were performed fully automatically using the same parameters setting for all 54 trees. Again, the

quantitative measurements described above were compared in different orientations.

3.3 Statistical Assessment

The reproducibility results are reported separately for the three phantom studies and for in vivo data. The average branchpoint positioning errors are only calculated for the computer phantom for which the true branchpoint positions were known. These errors are presented as mean \pm standard deviation and reported in voxels. All other reproducibility indices were compared using Bland-Altman statistic for which the average value of all corresponding measurements was used as an independent variable. The reproducibility showing 95% confidence intervals are presented in the form of Bland-Altman agreement plots [1].

4 Results

In the computer phantoms, the average branchpoint positioning error showed subvoxel accuracy of 0.93 ± 0.41 voxel size [10].

The reproducibility of the associated in the tree kinds of phantoms is discussed in [9,10].

The reproducibility of the quantitative tree morphology indices in in vivo CT scans are given in Fig. 7. In all cases, the relatively large differences between the surface and volume indices are to be expected due to a high sensitivity of these measures to minor partitioning errors, especially in short branches. Compare with the high reproducibility of the branch diameter and length measures.

5 Conclusion

The presented automated method for skeletonization, branchpoint identification and quantitative analysis of tubular tree structures is robust, efficient, and highly reproducible. It facilitates calculation of a number of morphologic indices described above as well as indices not considered in this work — branch angle, curvature, and many others.

The developed approach is built on the following novel concepts and skeletonization algorithm: fast curve-thinning algorithm to increase computational speed, endpoint re-checking to avoid generation of spurious side branches, depth-and-length sensitive pruning, exact tree-branch partitioning allowing branch volume and surface measurements, identification of non-branching tree segments, achieving sub-voxel accuracy of branch point positioning, and performing extensive validations on complex phantoms and in vivo scans.

Acknowledgments

This work was supported by the NIH grant HL-064368.

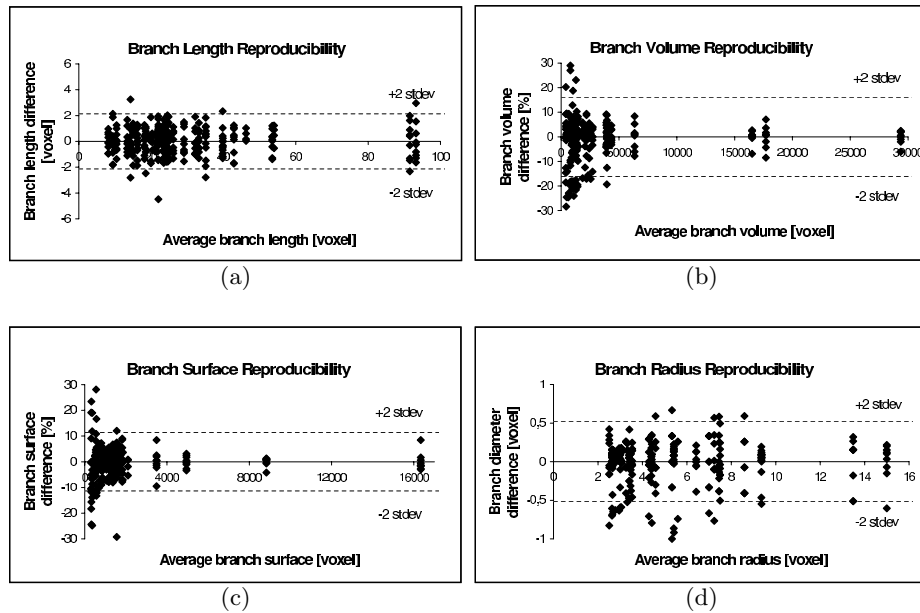


Fig. 7. Reproducibility in the 54 “reference” trees derived from in vivo CT data. a) Branch length, b) Branch volume, c) Branch surface area, and d) Average branch radius

References

1. J.M. Bland, D.G. Altman: Statistical methods for assessing agreement between two methods of clinical measurement. *Lancet* **1(8476)** (1986) 307–310
2. Z. Chen, S. Molloy: Automatic 3D vascular tree construction in CT angiography. *Computerized Medical Imaging and Graphics* **27** (2003) 469–479
3. G. Gerig, Th. Koller, G. Székely, Ch. Brechbühler, O. Kübler: Symbolic descriptions of 3-D structures applied to cerebral vessel tree obtained from MR angiography volume data, In: Proc. 13th Int. Conf. Information Processing in Medical Imaging, IPMI’93, Lecture Notes in Computer Science **687**, Springer (1993) 94–111
4. H. Kitaoka, R. Takaki, B.: A three-dimensional model of the human airway tree. *Journal of Applied Physiology* **87** (1999) 2207–2217
5. T.Y. Kong, A. Rosenfeld: Digital topology: Introduction and survey. *Computer Vision, Graphics, and Image Processing* **48** (1989) 357–393
6. M. Maddah, A. Afzali-Kusha, H. Soltanian-Zadeh: Efficient center-line extraction for quantification of vessels in confocal microscopy images. *Medical Physics* **30** (2003) 204–211
7. K. Mori, J. Hasegawa, Y. Suenaga, J. Toriwaki: Automated anatomical labeling of the bronchial branch and its application to the virtual bronchoscopy system. *IEEE Trans. Medical Imaging* **19** (2000) 103–114
8. I. Nyström: Skeletonization applied to magnetic resonance angiography images. Proc. Medical Imaging 1998: Image Processing, SPIE Vol. 3338 (2003) 693–701

9. K. Palágyi, J. Tschirren, M. Sonka: Quantitative analysis of three-dimensional tubular tree structures. In: Proc. Medical Imaging 2003: Image Processing, SPIE Vol. 5032 (2003) 277–287
10. K. Palágyi, J. Tschirren, M. Sonka: Quantitative analysis of intrathoracic airway trees: methods and validation. In: Proc. 18th Int. Conf. Information Processing in Medical Imaging, IPMI 2003, Lecture Notes in Computer Science 2732, Springer (2003) 222–233
11. J. Toriwaki, K. Mori: Distance transformation and skeletonization of 3D pictures and their applications to medical images. Digital and Image Geometry, Lecture Notes in Computer Science 2243, Springer (2001) 412–429
12. Y.F. Tsao, K.S. Fu: A parallel thinning algorithm for 3-D pictures. Computer Graphics and Image Processing **17** (1981) 315–331
13. S.Y. Wan, A.P. Kiraly, E.L. Ritman, W.E. Higgins: Extraction of the hepatic vasculature in rats using 3-D Micro-CT images. IEEE Trans. Medical Imaging **19** (2000) 964–971
14. S. Wood, A. Zerhouni, J. Hoford, E.A. Hoffman, W. Mitzner: Measurement of three-dimensional lung tree structures using computed tomography. Journal of Applied Physiology **79** (1995) 1687–1697